23rd International Conference on Renewable Energies and Power Quality (ICREPQ'25)
Tenerife (Spain), 25th to 27th June 2025
Renewable Energy and Power Quality Journal (RE&PQJ)
ISSN 2172-038 X, Volume No.23, September 2025

Evaluation of the sensitivity of measuring circuits for corona discharges detection

Milad Soltany[1], Jordi-Roger Riba[1] and Santiago Bogarra[1]

[1] Department of Electrical Engineering
AMBER High-Voltage Laboratory, Universitat Politècnica de Catalunya
Campus de Terrassa – 08222 Terrassa (Spain)

Abstract. Partial discharges (PD) play a major role in the degradation of insulation in high voltage equipment. PD occurs when localized electrical breakdowns occur in the presence of a high electric field near an insulator. A critical aspect of PD measurement is the calibration of the measurement system. Calibration results in a scale factor (k), that is used to convert the measured signal to the apparent charge. This paper presents a comparative analysis of five different measurement circuits used for PD detection. The experiments were performed using a sphere-to-plane configuration. In addition to the conversion factor, this study also examines the signal-to-noise ratio (SNR) for each measurement system.

Key words. Corona discharges, partial discharges, apparent charge, calibration, sensitivity.

1. Introduction

The IEC 60270 [1] defines the apparent charge $q_{apparent}$ of a PD pulse as the charge expressed in picocoulombs (pC) that, if injected between the two terminals of the device under test (DUT), would produce the same reading on the measuring instrument as that produced by the PD pulse. Since the actual charge involved in the discharge region, or physical charge, cannot be measured directly because the PD source is inaccessible [2], the apparent charge is measured instead, which is usually a small fraction of the the actual or physical charge. It should be noted that the apparent charge includes other effects such as those related to the measurement system itself, the capacitance of the experimental setup, and other external influences, so it does not uniquely represent the intrinsic behaviour of the insulation. When measuring partial discharges, since the PD source is not accessible, the transient voltage drop that occurs between the terminals of the device under test is detected [2].

According to [2], the apparent charge $q_{apparent}$ is indirectly proportional to the capacitance of the DUT C_{DUT}, which can be expressed as,

$$q_{apparent} = q_{true} C_{PDstray} / C_{DUT} \quad (1)$$

where $C_{PDstray}$ is the stray capacitance of the PD source. Therefore, for a fixed value of the true charge q_{true}, the measurable or apparent charge decreases as the DUT capacitance increases. This dependence also indicates that the apparent charge is not uniquely related to the PD intensity, but also to the characteristics of the DUT and the measurement system. In addition, $q_{apparent}$, i.e. the charge measurable across the terminations of the DUT is a small fraction of the q_{true} because of the stray capacitance of the PD, $C_{PDstray}$ is extremely small compared to the capacitance of the DUT, C_{DUT} ($C_{PDstray} << C_{DUT}$).

While PDs can occur in insulation systems based on solid, liquid or gaseous materials, when the PD occurs within a gaseous insulation such as atmospheric air, this type of discharge is typically known as a corona discharge [3], [4]. Corona discharges are characterized by pulses of approximately 1 μs duration or even less, and this phenomenon is accompanied by transient voltage drops across the terminals of the DUT, acoustic and electromagnetic emissions, UV and visible light, power losses, and generation of chemicals such as ozone or NOx [5].

Due to the low level energy involved in PD and corona discharges, especially in the early stages and near the corona inception voltage (voltage level at which continuous corona activity can be detected when the voltage is gradually increased from a very low voltage level [6]), it is of paramount importance to optimize the sensitivity of the measurement system.

This work describes and analyses the behaviour of different measurement circuits for the detection of corona discharges, and details the procedure for calibrating the PD generator and the circuit, while determining which of the circuits has more sensitivity and which has the best signal-to-noise ratio.

This work is organized as follows. Section 2 describes the calibration procedure. Section 3 provides full details of the proposed measurement circuits. Section 4 details the experimental setup. Section 5 presents and discusses the results obtained. Finally, Section 6 concludes this work.

2. Calibration procedure

Both the PD pulse generator (PG) and the circuit must be calibrated because each circuit has a specific response to a PD pulse injected between the terminals of the device under test (DUT).

A Calibration of the PD pulse generator

Before initiating any partial discharge (PD) calibration process, it is essential to ensure that PD generators are periodically calibrated using procedures traceable to national/international standards. The conventional approach to calibrating a PD calibrator is to inject a known charge and determine it by numerically integrating the current flowing through a resistor placed between the calibrator output and ground. This method, known as the numerical integration technique, is typically used for charges above 20 pC, although it remains effective for charge levels above 10 pC because the signal-to-noise ratio (SNR) of the measurement is directly proportional to the applied charge. However, at very low charge levels, measuring millivolt level signals with high accuracy presents significant challenges due to the limitations of digitizers in capturing weak signals with minimal noise interference.
The charge from the PD calibrator is injected into a resistor connected in parallel with the high-impedance input of the digitizer (in our case the oscilloscope), as shown in Figure 1. The current $i(t)$ flowing through the resistor can be determined by dividing the measured voltage $u(t)$ by the value R of the resistor. The charge of the pulse q_{pulse} can then be obtained by numerically integrating the current as,

$$q_{pulse} = \int_{t_1}^{t_2} i(t)dt = \int_{t_1}^{t_2} [u(t)/R]dt \qquad (2)$$

Figure 1 shows the PD pulse generator (PG) calibration circuit recommended in IEC 60270 standard [1].

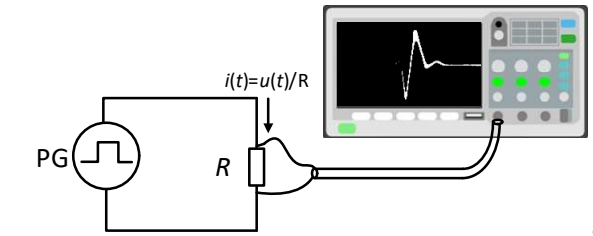

a)

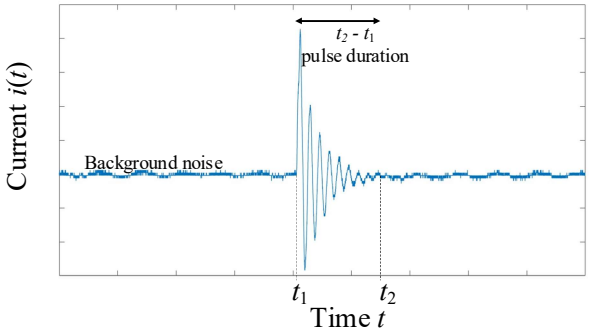

b)

Figure 1. Test circuit used to calibrate the PD pulse generator.

B. Calibration of the circuit

The calibration procedure is based on injecting a pulse of known charge $q_{injected}$ [pC] between the two terminals of the DUT using a PD pulse generator (PG) and measuring the charge at the side of the measuring system $q_{measured}$ [pC], as shown in Figure 2a. The calibration constant K_{cal} can then be calculated as,

$$K_{cal} = \frac{q_{measured}}{q_{injected}} = \frac{\int_{t_1}^{t_2} [u(t)/R_{50\Omega}]dt}{q_{injected}} \qquad (3)$$

where $q_{injected}$ [pC] is the charge injected by the calibrator, $q_{measured}$ [pC] the measured charge which can be determined by integrating the voltage detected by the sensor $u(t)$ [V] divided by the input resistance $R_{50\Omega}$ [Ω] of the measurement system over the duration of the pulse, $t_{pulse} = t_2 - t_1$ [s]. Note that a non-inductive resistor is used for this purpose.

When performing PD measurements, it is also important to know the background noise level, as it can greatly affect the sensitivity of the measurement. It can be measured as shown in Figure 2b. Note that the circuit shown in Figure 2 uses a coupling capacitor (CC) and a measuring impedance (MI) in parallel with the DUT.

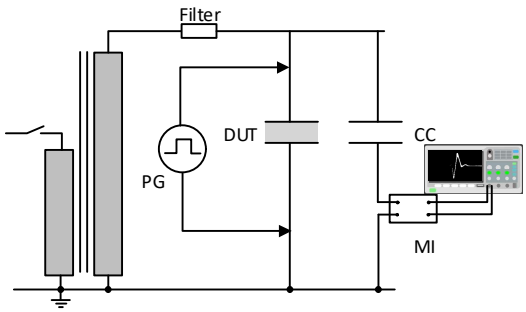

a)

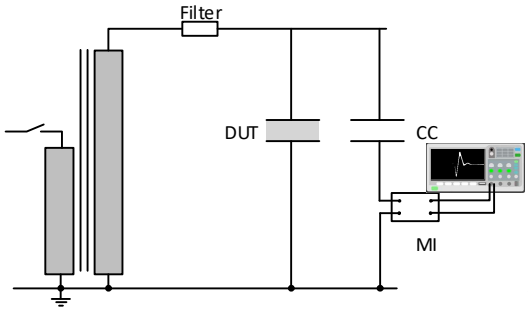

b)

Figure 2. a) Circuit calibration. b) Background noise level measurement.

The background noise level can be characterized by the signal-to-noise ratio (SNR), which can be defined as the ratio between the root mean square (RMS) value of the PD pulse voltage $u_{RMS,PDpulse}$, and the RMS value of the background noise $u_{RMS,noise}$ as,

$$SNR = \frac{u_{RMS,PDpulse}}{u_{RMS,noise}} \qquad (4)$$

3. Proposed measurement circuits

Several circuits have been used to determine the calibration constant, as shown in Figure 3. Note that all the circuits use a 1000 pF coupling capacitor (CC) and some of them use an HFCT and some use a measuring impedance (MI).

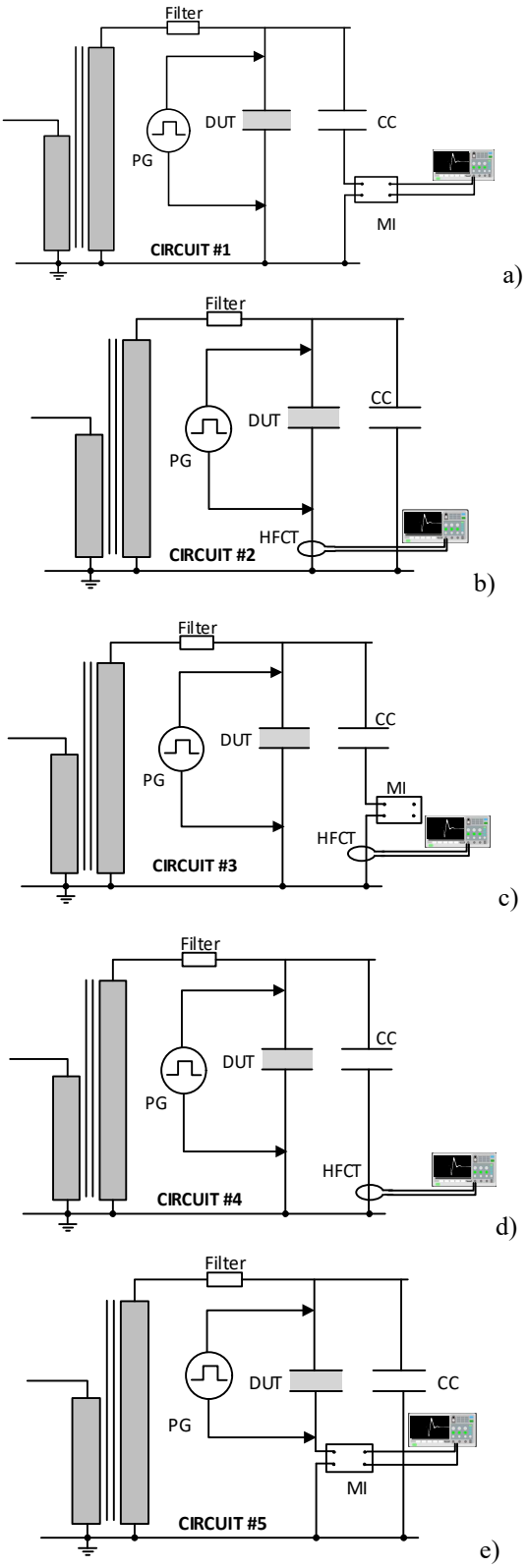

Figure 3. Different circuits used for sensitivity comparison.

4. Experimental setup

This section describes the experimental setup used in the experiments, which is shown in Figure 4.

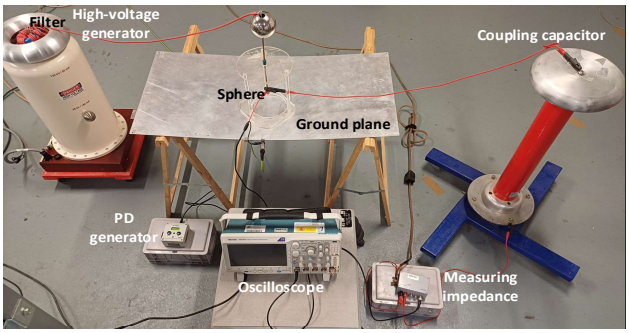

Figure 4. Photograph of the experimental setup.

A BK130/36 50 Hz AC generator was used to generate a variable high voltage. To minimize the noise level, two filters were used, one on the low voltage side of the generator and another on the high voltage side. A TE Connectivity 10VN1 single-phase EMC/EMI line filter was used in the low voltage side of the HV generator. The high voltage side filter consists of 32 turns wound on a TDK Electronics epoxy N30 ferrite toroidal core with an outer diameter of 102 mm, an inner diameter of 65.8 mm and a height of 15 mm, with a total inductance of 5.1 mH.

A Techimp PDCAL PD generator with scales of 1-2-5-10-20-30-50-70-100 pC was used during the calibration phase of the experiments.

A CPL542 measuring impedance (MI) from Omicron (20 kHz - 6 MHz) was used to optimize the sensitivity of the measurement system.

An MCT 120 high-frequency current transformer (HFCT) was also used for PD measurements (Omicron, frequency range -6 dB: 80 kHz to 40 MHz, 53.5 mm inside diameter).

A Tektronix MDO324 oscilloscope (200 MHz, 2.5 GS/s per channel, > 280,000 wfm/s per channel, 11-bit vertical resolution in high resolution mode) connected to the MI or HFCT via a coaxial BNC cable (100 cm, military grade MIL-DTL-17 manufactured by Coleman) was used to acquire the PD waveforms.

A sphere-plane configuration was used because it is easy to implement and is widely used in high-voltage engineering [7], [8]. A 14.5 mm diameter stainless steel sphere was used and placed 100 mm above a metallic ground plane (bottom of sphere to plane).

5. Results

A. Calibration of the PD generator

This section shows the results of calibrating the PD generator.

As explained in Section 2, it is important to ensure that the PG is already generating pulses with the correct charge. Table I summarizes the results obtained during the calibration of the PG, which was set to four scales, i.e. 100 pC, 70 pC, 50 pC and 30 pC. It should be noted that 30 pulses were acquired for each scale, and μ [pC] is the mean and σ [pC] is the standard deviation of the pulses for each scale.

Table I. Pulse generator calibration results

$q_{injected}$ [pC]	Measured values	
	μ [pC]	σ [pC]
100	95	0.9
70	66	0.8
50	47	0.8
30	29	0.6

The results in Table I show that there is some dispersion in the pulses generated by the PG, so when calibrating it is necessary to acquire many pulses to obtain a good average.

B. Calibration of the different measurement circuits

This section shows the results of the calibration performed on the five measurement circuits described in Section 3. Table II summarizes the results obtained when calibrating the different circuits shown in Figure 3. It should be noted that each row corresponds to the mean value of 30 samples.

Table II. Calibration results of the five analysed measurement circuits

Circuit number	$q_{injected}$ [pC]	$v(t)$ [mV$_{RMS}$]	$v_{noise}(t)$ [mV$_{RMS}$]	$q_{measured}$ [pC]	K_{cal}	SNR
#1	95	10.83	0.64	40	0.42	17.09
	66	8.64	0.65	28	0.42	13.41
	47	7.04	0.74	20	0.44	9.56
	29	4.38	0.65	13	0.47	6.70
#2	95	8.07	0.58	8	0.08	14.06
	66	6.11	0.56	4	0.06	10.87
	47	4.75	0.53	3	0.08	8.90
	29	2.91	0.53	2	0.09	5.47
#3	95	5.99	0.70	8	0.08	8.61
	66	4.30	0.75	6	0.09	5.74
	47	3.11	0.76	5	0.10	4.08
	29	2.17	0.75	4	0.13	2.9
#4	95	9.40	0.83	6	0.06	11.37
	66	6.99	0.73	4	0.05	9.66
	47	5.06	0.73	3	0.07	6.97
	29	3.10	0.75	3	0.1	4.11
#5	95	12.43	0.62	41	0.43	20.14
	66	8.80	0.59	30	0.45	14.93
	47	6.34	0.57	23	0.49	11.17
	29	4.22	0.55	14	0.49	7.71

The results presented in Table II show that Circuit #5 is the one with the higher SNR and higher sensitivity since it has the higher K_{cal} value. However, care must be taken when using Circuit #5 because the MI is placed in the direct path between the DUT and ground, so any spurious discharge could damage the MI and the oscilloscope. Note that when using the HFCT, the most sensitive results are obtained when it is connected in series with the coupling capacitor and measuring impedance (Circuit #3), while the higher SNR values correspond to Circuit #2.

6. Conclusion

Partial discharges and corona discharges produce very low-level pulses of very short duration, especially near the inception point. Therefore, it is not easy to detect such low energy pulses, being very important to optimize the sensitivity and the signal to noise ratio of the measurement system. This paper has focused on analysing the sensitivity and the signal to noise ratio of different circuits for partial discharge measurements. It has been shown that Circuit #1 (MI in series with the CC) is the one that better protects the measurement devices against accidental discharges, while Circuit #5 (MI in series with the DUT and with a CC in parallel with the DUT + MI) is the one with the best sensitivity and SNR.

Acknowledgement

This project received funding from grant PID2023-147016OB-I00,by MICIU/AEI/10.13039/501100011033/ and by ERDF "A way of making Europe," by the European Union and from the Agència de Gestió d'Ajuts Universitaris i de Recerca-AGAUR (2021 SGR 00392).

References

[1] International Electrotechnical Commission, *IEC 60270:2000 High-voltage test techniques - Partial discharge measurements*, 3.0. International Electrotechnical Commission, 2000.

[2] Eberhard Lemke *et al.*, "Guide for electrical Partial Discharge Measurements in compliance to IEC 60270," *Electra*, vol. 241, no. Technical Brochure 366, pp. 61–67, 2008.

[3] J.-R. R. Riba, "Linking digital image intensity to carrier density in low-pressure corona discharges," *Sensors Actuators A Phys.*, vol. 359, p. 114474, 2023.

[4] J.-R. Riba, C. Abomailek, P. Casals-Torrens, and F. Capelli, "Simplification and cost reduction of visual corona tests," *IET Gener. Transm. Distrib.*, vol. 12, no. 4, pp. 834–841, Feb. 2018.

[5] C. Abomailek, J.-R. Riba, and P. Casals-Torrens, "Feasibility analysis of reduced-scale visual corona tests in high-voltage laboratories," *IET Gener. Transm. Distrib.*, vol. 13, no. 12, pp. 2543–2549, 2019.

[6] IEEE, "IEEE Std 100-2000 The Authoritative Dictionary of IEEE Standards Terms, Seventh Edition," *IEEE Std 100-2000*. pp. 1–1362, 2000.

[7] P. Bas-Calopa, J.-R. Riba, and M. Moreno-Eguilaz, "Measurement of Corona Discharges under Variable Geometry, Frequency and Pressure Environment,"

Sensors 2022, Vol. 22, Page 1856, vol. 22, no. 5, p. 1856, Feb. 2022.

[8] S. I. Wais and D. D. Giliyana, “Sphere-to-Plane Electrodes Configuration of Positive and Negative Plasma Corona Discharge,” *Am. J. Mod. Phys.*, vol. 2, no. 2, pp. 46–52, 2013.